NASA TECHNICAL NOTE

NASA TN D-
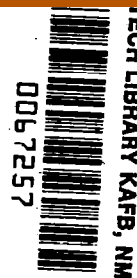
NASA TN D-4392

COLD-AIR PERFORMANCE EVALUATION OF SCALE MODEL OXIDIZER PUMP-DRIVE TURBINE FOR THE M-1 HYDROGEN-OXYGEN ROCKET ENGINE

III - Performance of First Stage With Inlet-Feedpipe-Manifold Assembly

by Roy G. Stabe and John F. Kline

Lewis Research Center

Cleveland, Ohio
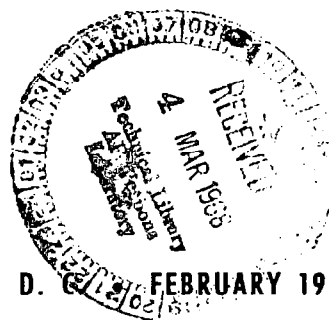
NATIONAL AERONAUTICS AND SPACE ADMINISTRATION • WASHINGTON, D. C. • FEBRUARY 1968

COLD-AIR PERFORMANCE EVALUATION OF SCALE MODEL OXIDIZER

PUMP-DRIVE TURBINE FOR THE M-1 HYDROGEN-OXYGEN

ROCKET ENGINE

III – Performance of First Stage With Inlet-Feedpipe-

Manifold Assembly

By Roy G. Stabe and John F. Kline

Lewis Research Center
Cleveland, Ohio

NATIONAL AERONAUTICS AND SPACE ADMINISTRATION

COLD-AIR PERFORMANCE EVALUATION OF SCALE MODEL OXIDIZER PUMP-

DRIVE TURBINE FOR THE M-1 HYDROGEN-OXYGEN ROCKET ENGINE

III - PERFORMANCE OF FIRST STAGE WITH INLET-FEEDPIPE-

MANIFOLD ASSEMBLY

by Roy G. Stabe and John F. Kline

Lewis Research Center

SUMMARY

The aerodynamic performance of the first stage of a 0.45-scale model of the oxygen pump-drive turbine for the M-1 rocket engine was determined experimentally. The first stage, including the inlet-feedpipe-manifold assembly, was tested over a range of speeds and pressure ratios. The working fluid used in the investigation was dry air at inlet total conditions of 600° R (333° K) and approximately atmospheric pressure.

The results of the investigation indicated that, at design equivalent speed and blade-jet speed ratio, the first-stage static and total efficiencies were very close to design values. The static and total efficiencies were 0.37 and 0.57 compared with the design values of 0.375 and 0.563, respectively. The equivalent weight flow at the design point was the same as that reported for the reference two-stage turbine investigation, that is, 6.31 pounds per second (2.86 kg/sec) or 10.8 percent less than the design value of 7.071 pounds per second (3.20 kg/sec). The weight flow was reduced by a higher-than-design inlet-manifold total-pressure loss, a large circumferential variation in manifold flow conditions, and a 3.7-percent deficit in nozzle throat area. In addition, the rotor throat area was 9 percent less than design. The less-than-design throat areas changed the static-pressure distribution from design and reduced the nozzle-exit velocity. This change caused a further reduction in the weight flow.

Results of a velocity diagram and a loss analysis of the first-stage performance indicated that the rotor efficiency was essentially as designed, 0.81 compared with the design value of 0.80. The nozzle performed better than design; the nozzle efficiency was 0.94 compared with the design value of 0.91. This improved nozzle performance counterbalanced the high manifold loss. As a result, the overall efficiency of the manifold-nozzle combination was essentially as designed. The velocity diagrams computed from test data differed somewhat from design. The nozzle exit and rotor-exit flow angles were greater than design principally because of the small nozzle and rotor throat areas. In addition, the reaction across the rotor was higher than design, also because of the small rotor throat area.

INTRODUCTION

Experimental performance evaluations of the pump-drive turbines for the M-1 engine are included as part of the turbine research and project support programs. The M-1 is a 1.5-million-pound-thrust (6.67×10^6 N-thrust) hydrogen-oxygen rocket engine. Fuel and oxidizer turbopumps are mounted on opposite sides of the engine combustion chamber. Each pump is driven by a two-stage velocity-compounded turbine.

Details of the fuel pump-drive turbine design are given in reference 1. Cold-air performance evaluations of a 0.646-scale-model, fuel-turbine, inlet-feedpipe-manifold assembly, first-stage, and complete two-stage turbine are reported in reference 2. Details of the oxygen pump-drive turbine design are given in reference 3. An investigation of a 0.45-scale model of this turbine was also made and included an experimental determination of the inlet manifold-nozzle performance (ref. 4) and an experimental determination of the two-stage turbine performance (ref. 5).

In reference 4, it is reported that the comparatively high velocities in the inlet feedpipes and manifold caused a larger-than-design loss in manifold total pressure and a substantial circumferential variation in nozzle-exit flow conditions. Also, the weight flow was 10.2 percent less than design at design pressure ratio. The reduction in weight flow was attributed to a 3.7-percent deficit in the nozzle throat area, the larger-than-design manifold total pressure loss, and the circumferential variation in manifold flow conditions.

In reference 5, it is reported that the static efficiency of the two-stage turbine approached the design value but that the two-stage turbine did not operate with the design axial or radial distribution of static pressure. This nondesign static-pressure distribution caused a further reduction in the weight flow. At design equivalent speed and pressure ratio, the equivalent weight flow was 10.8 percent less than design.

An experimental investigation of the first stage of the 0.45-scale-model turbine was undertaken to better define several aspects of the oxygen pump-drive turbine performance. The reasons for the weight flow deficit, the performance of the blading, and the influence of the inlet manifold on the turbine performance were of particular interest. This report presents the results of the cold-air performance evaluation of this first stage, including the inlet-feedpipe-manifold assembly. The turbine was tested at constant speeds of 60, 80, 90, 100, and 110 percent of design equivalent speed and over a range of pressure ratios from 1.2 to 2.0. Zero-speed torque data were also obtained. First-stage performance in terms of weight flow, specific work, static efficiency, torque, and static pressures is presented for the range of speeds and pressure ratios covered in the investigation. The results of radial surveys of rotor-exit flow conditions and of an analysis to determine the magnitude of the various losses at design equivalent speed and pressure ratio are also included.

SYMBOLS

c_p specific heat at constant pressure, Btu/(lb)(^{O}R); J/(kg)(^{O}K)

g_c dimensional conversion constant, 32.17 ft-lb/(lb)(sec^2)

h specific enthalpy, Btu/lb; J/jg

$\Delta h'$ turbine specific work, Btu/lb; J/kg

J mechanical equivalent of heat, 778 ft-lb/Btu

N rotative speed, rpm

p absolute pressure, lb/in.^{2}; N/m^2

R gas constant, ft-lb/(lb)(^{O}R); J/(kg)(^{O}K)

r radius, in.; m

T temperature, ^{O}R; ^{O}K

U blade speed, ft/sec; m/sec

V absolute velocity, ft/sec; m/sec

W velocity relative to rotor blade, ft/sec; m^2

w weight flow, lb/sec; kg/sec

α absolute flow angle measured from axial direction, deg

β relative flow angle measured from axial direction, deg

γ ratio of specific heats

δ ratio of inlet total pressure to U.S. standard sea-level atmospheric pressure, pressure, $p_1'/(14.696$ lb/in.^{2}); $p_1'/(101\ 325$ N/m^2)

ϵ gamma correction function, $\left(\dfrac{0.74}{\gamma}\right)\left(\dfrac{\gamma + 1}{2}\right)^{\gamma/(\gamma-1)}$

η turbine static efficiency, $\Delta h'/\left(h_1' - h_4\right)_s$

$\sqrt{\theta_{cr,1}}$ ratio of turbine-inlet critical velocity to critical velocity of U.S. standard sea-level air, $V_{cr,1}/(1019$ ft/sec); $V_{cr,1}/(310.6$ m/sec)

ν blade-jet speed ratio, $U_m\Big/\sqrt{2g_c J\left(h_1' - h_4\right)_s}$; $U_m\Big/\sqrt{2\left(h_1' - h_4\right)_s}$

3

τ torque, lb-ft; N-m

Subscripts:

cr   condition corresponding to those at Mach number of 1

h   blade-hub section

s   isentropic or ideal process

t   blade-tip section

1, 2, 3, 4, 4a   measuring stations (see fig. 2)

Superscripts:

-          average value

'   absolute total condition

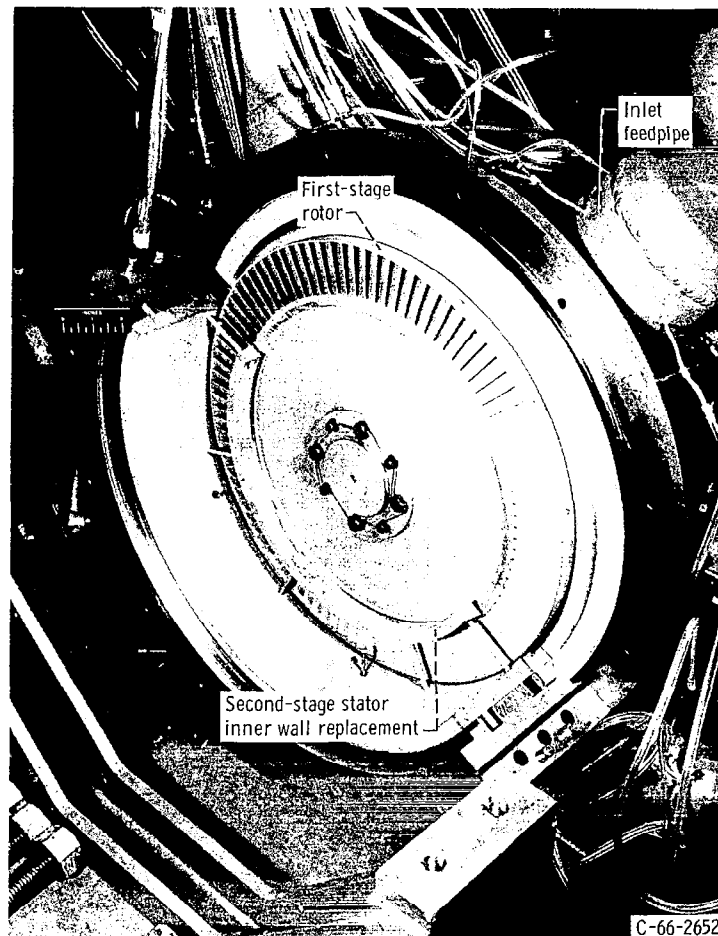''   total state condition relative to rotor blade

Figure 1. - Turbine assembly with part of casing removed (upstream view).

APPARATUS AND PROCEDURE

The 0.45-scale model with which the performance of the complete M-1 oxidizer pump-drive turbine was evaluated (ref. 5) was used for the present investigation. The second-stage rotor was removed, and the second-stage stator was replaced with a fixture having similar inner and outer walls (but no blades). The test turbine assembly with half the casing removed is shown in figure 1.

The aerodynamic design specifications for this configuration (manifold assembly and first stage) of the full-scale turbine are presented in table I. The equivalent specifications for operation with U.S. standard sea-level air for the 0.45-scale model are also shown. These specifications are based on the design total temperature and pressure in the inlet feedpipes (see refs. 3 and 4). The working fluid properties used to determine the equivalence conversions are presented in table II. The design mean-diameter velocity diagrams are shown in figure 2.

TABLE I. - AERODYNAMIC DESIGN CONDITIONS FOR FIRST STAGE [a]

Parameter	Hydrogen-oxygen combustion products		U.S. standard sea-level air equivalent conditions		
	Symbol	Full size	Symbol	Full size	0.45 Scale
Inlet total temperature:	T_1'		T_1'		
°R		1190		518.7	518.7
°K		661		288.2	288.2
Inlet total pressure:	p_1'		p_1'		
psia		208.1		14.696	14.696
N/m^2		1.435×10^6		101 325	101 325
Weight flow:	w		$\frac{w\epsilon}{\delta}\sqrt{\theta_{cr,1}}$		
lb/sec		115		34.92	7.071
kg/sec		52.16		15.84	3.207
Speed:	N		$N/\sqrt{\theta_{cr,1}}$		
rpm		3635		852	1893
Specific work:	Δh'		$\Delta h'/\theta_{cr,1}$		
Btu/lb		113.1		6.214	6.214
J/kg		262 800		14 440	14 440
Torque:	τ		$\tau\epsilon/\delta$		
lb-ft		26 550		1888	172
N-m		35 996		2560	233
Pressure ratio	$p_1'/\overline{p}_4$	1.641	$p_1'/\overline{p}_4$	1.646	1.646
Blade-jet speed ratio	ν	0.135	ν	0.135	0.135
Static efficiency	η	0.375	η	0.375	0.375

[a]Includes inlet-manifold and feedpipe parameters.

TABLE II. - THERMODYNAMIC PROPERTIES OF

WORKING FLUID

Property	Hydrogen-oxygen combustion products	U.S. standard sea-level air
Specific heat, c_p:		
Btu/(lb)(^{O}R)	1.98	0.24
J/(kg)(^{O}K)	8284	1004
Ratio of specific heats, γ	1.382	1.4
Gas constant, R:		
ft-lb/(lb)(^{O}R)	425.8	53.35
J/(kg)(^{O}K)	2291	287
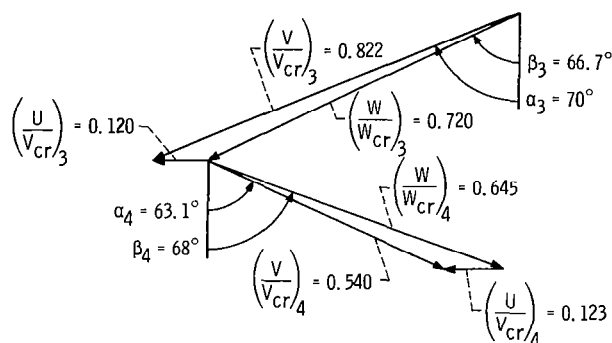
Figure 2. - Design first-stage mean-diameter velocity diagram.

The test facility was substantially the same as that used for the complete turbine. A diagram and an overall view are shown in figure 3.
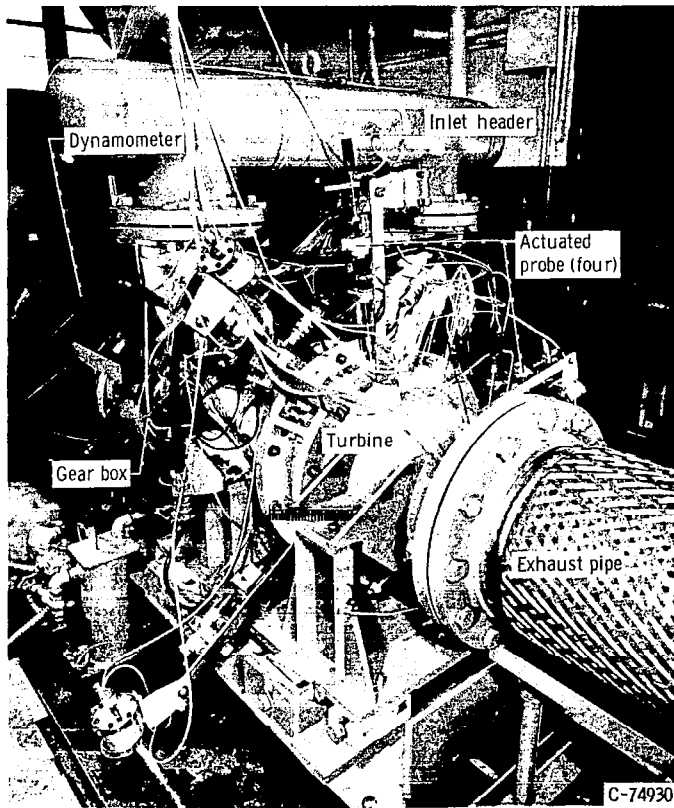
The axial and circumferential location of the instrumentation is shown in figure 4. The instrumentation in the feedpipe, manifold, and nozzle was the same as that used in the two-stage tests, except that wall static-pressure taps were added at 14 circumferential positions around the hub of the inlet manifold (station 2). Hub and tip wall static-pressure taps were installed at five circumferential positions at station 4 in the stator wall replacement fixture. Station 4 was at the same axial location as for the two-stage tests. Four actuated combination (total-pressure and flow-angle) radial survey probes were located around the circumference 1 blade chord downstream from the rotor exit (station 4a). Figure 5 is a view looking upstream at the rotor exit with the stator wall fixture and the survey probes in position.

Air-flow rate was measured with a calibrated ASME thin-plate orifice run. Orifice inlet pressure was measured with a calibrated precision Bourdon tube gage. All other pressures were recorded simultaneously by photographing a bank of mercury fluid manometers. Temperatures were read on an industrial self-balancing potentiometer.

Inlet

Header

Feedpipes

Exhaust

Cradled gearbox

Direct-current electric
dynamometer

Force cell

Turbine test section

CD-8303
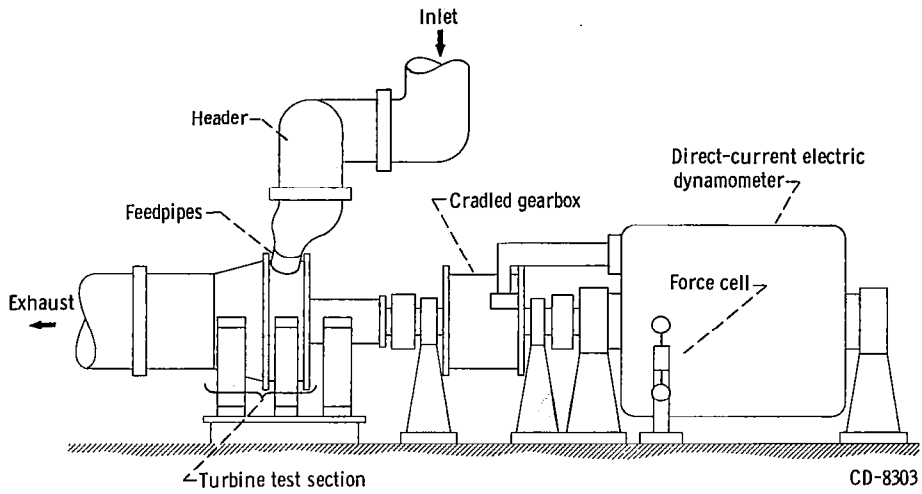
(a) Schematic diagram.

Figure 3. - Turbine test facility.

Dynamometer

Inlet header

Actuated
probe (four)

Turbine

Gear box

Exhaust pipe
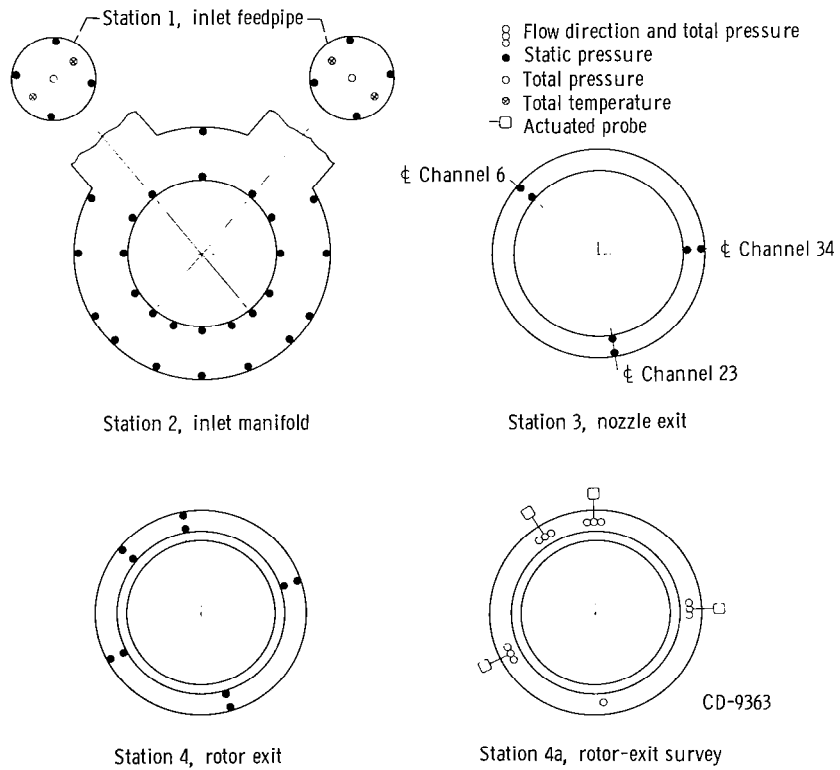
C-74930

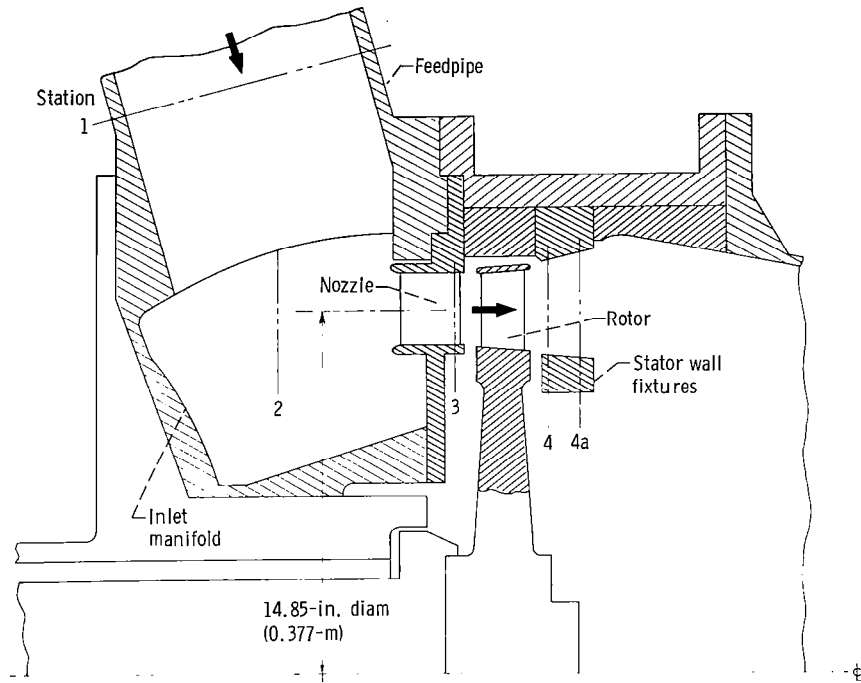(b) Turbine installation.

Figure 3. - Concluded.

7

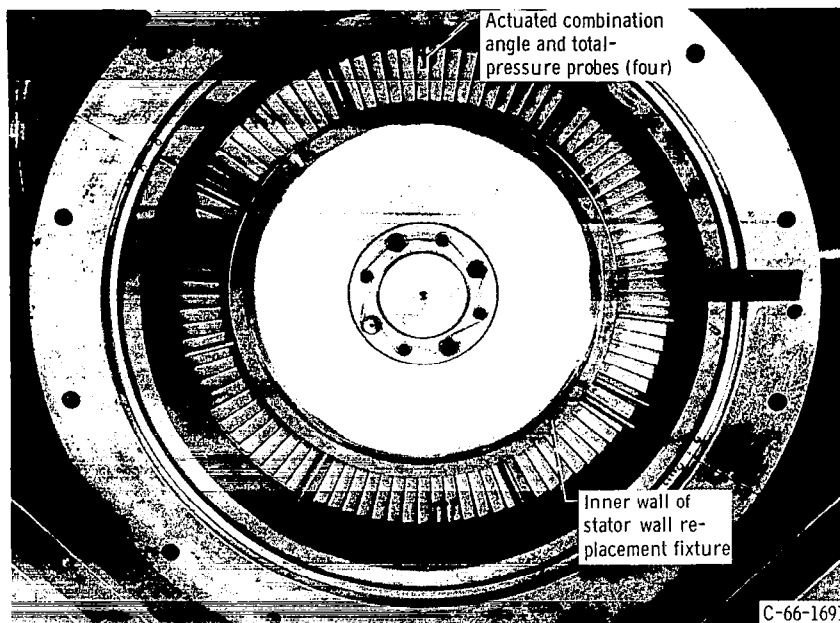Figure 4. - Station nomenclature and location of instrumentation. (All views looking upstream.)

Figure 5. - Rotor-exit instrumentation.

Turbine rotative speed was measured with an electronic counter in conjunction with a magnetic pickup and a 60-tooth gear mounted on the turbine shaft. Output power was transmitted through a cradled gear box and absorbed by a cradled direct-current dynamometer. The total reaction torque of the gearbox and dynamometer was measured with a strain-gage force cell in conjunction with an integrating digital millivoltmeter. This system was calibrated in place before and after each day's operation by deadweight loading of the dynamometer stator.

The turbine was operated with dry air at a total pressure of 30 inches of mercury absolute (101 580 N/m^2) and a total temperature of 600° R (333° K) at station 1 in the manifold feedpipes. Data were taken at rotative speeds of 0, 60, 80, 90, 100, and 110 percent of design equivalent speed and at pressure ratios (inlet total to exit static) from approximately 1.2 to 2.0. Bearing-seal torque was determined directly by removing the rotor and motoring the test unit at each speed. Rotor-exit flow angle and total pressure were surveyed at design equivalent speed and pressure ratio.

Turbine specific work $\Delta h'$ was calculated from weight flow, speed, and turbine torque data. Turbine torque was determined by adding bearing-seal torque (approximately 2 percent of design first-stage torque) to the torque indicated by the force cell. Turbine performance is based on the pressure ratio determined by the calculated inlet total pressure p_1' and the average of the hub and tip static pressures $\bar{p}_4$ measured at station 4. Inlet total pressure p_1' is the average total pressure calculated from the average static-pressure, temperature, and flow area at station 1 in the feedpipes and the turbine weight flow.

9

RESULTS AND DISCUSSION

The first-stage turbine configuration was tested at constant speeds of 0, 60, 80, 90, 100, and 110 percent of design equivalent speed and over a range of pressure ratios from approximately 1.2 to 2.0. The test configuration included the inlet manifold assembly, and the performance data presented in the following section includes the losses attributable to this assembly.

Weight Flow

Equivalent weight flow is plotted against equivalent pressure ratio and speed in figure 6. At design equivalent pressure ratio and speed, the equivalent weight flow was 6.31 pounds per second (2.86 kg/sec), which is 10.8 percent less than the design value of 7.071 pounds per second (3.20 kg/sec). This value is the same as the equivalent weight flow reported for the two-stage turbine in reference 5. These results indicate
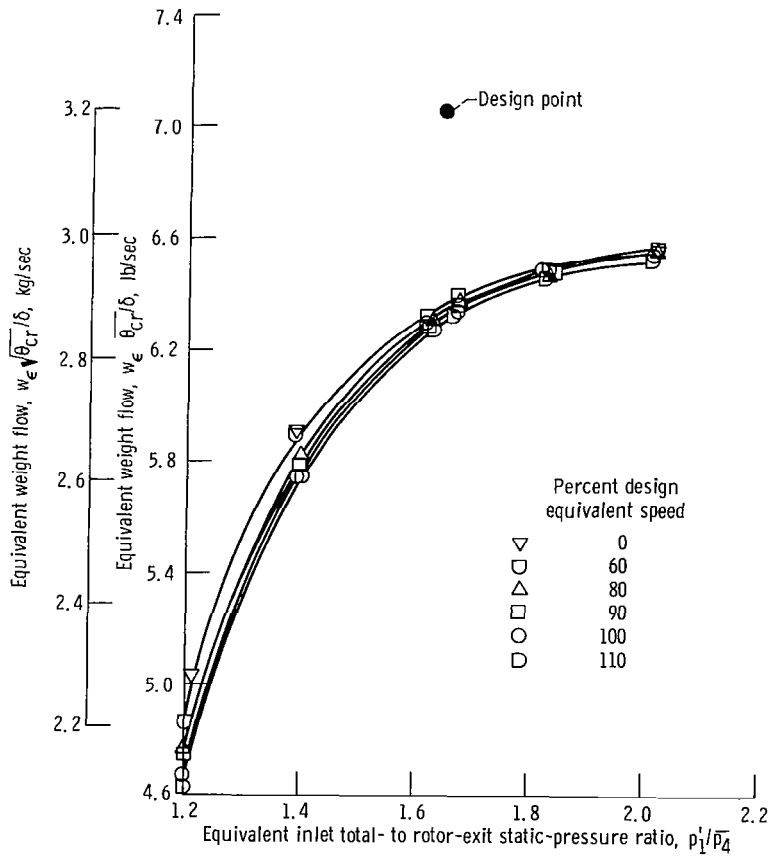
Figure 6. - Variation of equivalent weight flow with pressure ratio and speed.

that the nozzle operated at the same pressure ratio in both one- and two-stage turbine configurations.

As discussed in the INTRODUCTION, the weight flow was reduced by the large circumferential variation in manifold flow conditions, by the higher-than-design inlet manifold total pressure loss, and also by the 3.7-percent deficit in nozzle throat area. In addition, the first-stage rotor throat area was 9 percent less than design. Both the nozzle and the first-stage rotor were built with larger-than-design blade angles, which reduced the throat areas. The nozzle blade angle was approximately 0.6° larger than design, and the rotor blade angle was approximately 2° larger than design. The less-than-design-throat areas caused changes in the static-pressure distribution and resulted in a further reduction in the flow. These effects are discussed in more detail in subsequent sections.

Equivalent Specific Work

Equivalent specific work as a function of equivalent pressure ratio and speed is shown in figure 7. At design equivalent speed and pressure ratio, the equivalent specific work is 6.15 Btu per pound (14 300 J/kg), approximately 1 percent less than the design value of 6.214 Btu per pound (14 400 J/kg). The continued upward trend of the equivalent specific-work curves at the higher pressure ratios indicates that the first stage was not operating near limiting loading.
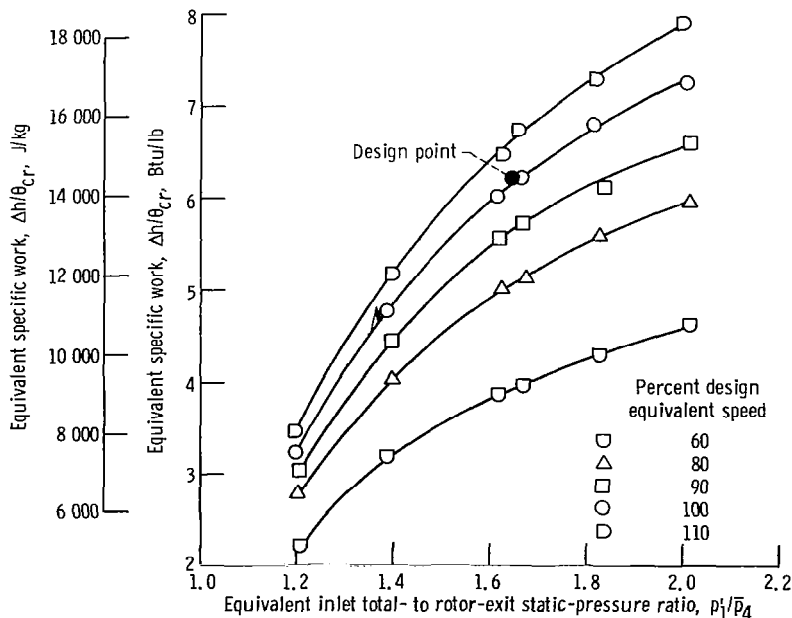

Figure 7. - Variation of first-stage equivalent specific work with pressure ratio and speed.
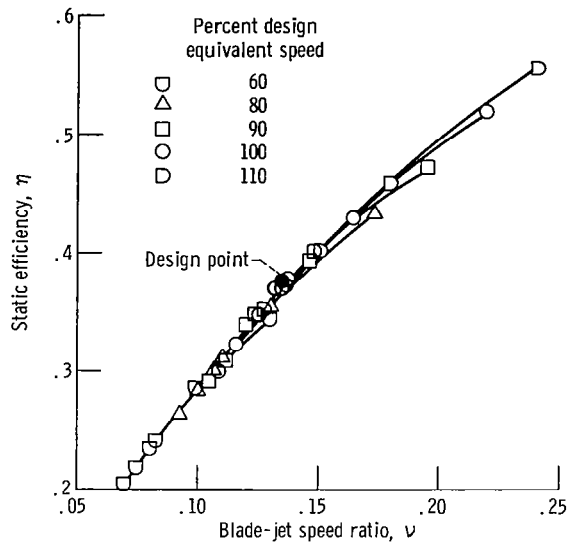
Figure 8. - Variation of first-stage static efficiency with blade-jet speed ratio and speed.
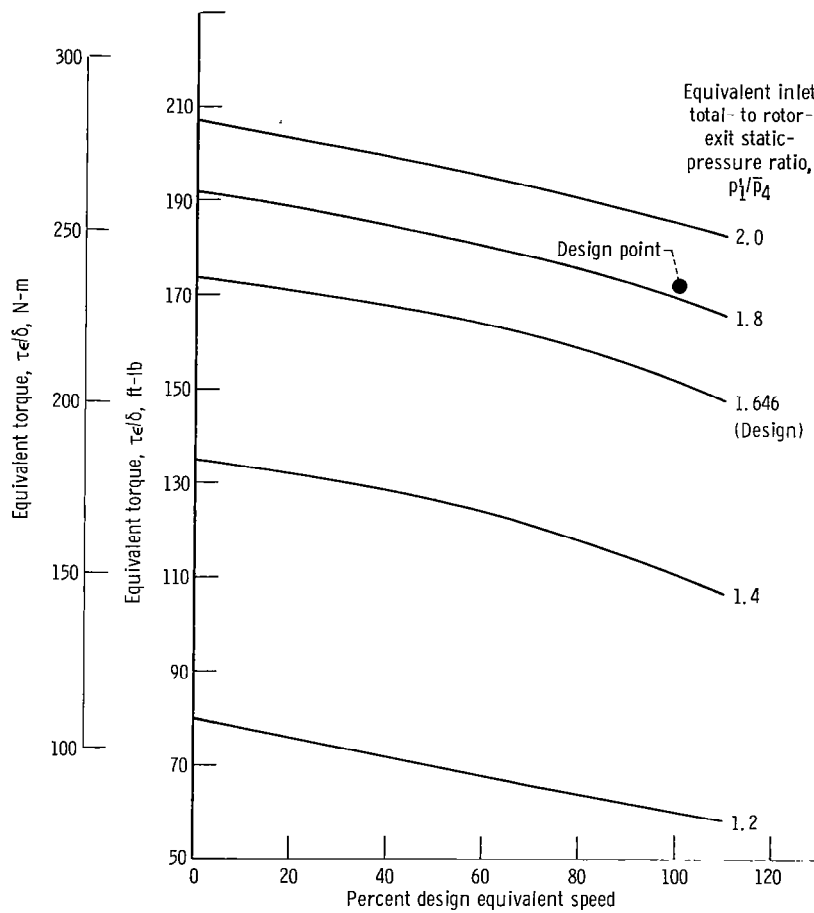

Figure 9. - Variation of first-stage equivalent torque with speed and pressure ratio.

Static Efficiency

First-stage static efficiency as a function of blade-jet speed ratio and percent design equivalent speed is shown in figure 8. The static efficiency of the first stage was very nearly equal to the design value. At first-stage design speed and blade-jet speed ratio (0.135), the static efficiency was 0.37 as compared with 0.375 design.

Equivalent Torque

Equivalent torque as a function of percent design equivalent speed and pressure ratio is shown in figure 9. These curves were constructed from plots of equivalent torque against equivalent pressure ratio for constant speeds of 0, 60, 80, 90, 100, and 110 percent of design equivalent speed.

The equivalent torque at first-stage design equivalent speed and pressure ratio is 152 pound-feet (206 N-m), which is 11.6 percent less than the design value of 172 pound-feet (233 N-m). The largest part of this deficit is due to the lower-than-design weight flow and the balance to the slightly less-than-design static efficiency. At first-stage design equivalent inlet total- to exit static-pressure ratio, the ratio of zero speed to design-speed equivalent torque is approximately 1.14. This ratio is small because of the very low first-stage blade-jet speed ratio (0.135).
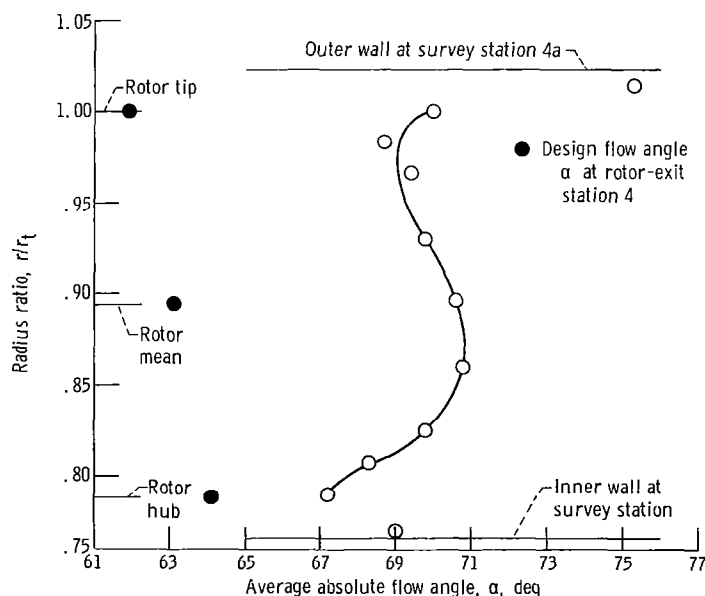

Figure 10. – Radial variation of first-stage rotor-exit flow angle at design equivalent speed and approximately design equivalent pressure ratio.

Rotor-Exit Surveys

Radial surveys of first-stage rotor-exit flow conditions were taken at design equivalent speed and nominally design equivalent inlet total- to exit static-pressure ratio. The absolute flow angle and total pressure were measured at four circumferential positions and at several radial locations along the blade span.

The radial variation in the first-stage rotor-exit flow angle is shown in figure 10. The data shown in figure 10 represent the circumferential average of the four measurements taken at each radial location. Both the magnitude and the radial variation of the exit angle differ from the design hub, mean, and tip design values shown. The spanwise-integrated average flow angle is 69.8° as compared with the mean-diameter design value of 63.1°.

The principal reasons for the larger-than-design rotor-exit flow angle were the larger-than-design blade angle and the less-than-design weight flow. The less-than-design weight flow results in a decrease in the axial velocity, which increases the exit flow angle.

The radial variation of the first-stage average rotor-exit total-pressure ratio $\bar{p}_4'/p_1'$ is shown in figure 11. The minimum value of the rotor-exit to rotor-inlet total-pressure ratio of 0.690 occurs at the tip diameter and the maximum ratio of 0.735 occurs near the mean diameter. The spanwise-integrated average rotor-exit to rotor-inlet total-pressure ratio is 0.724, very near the design value of 0.723.
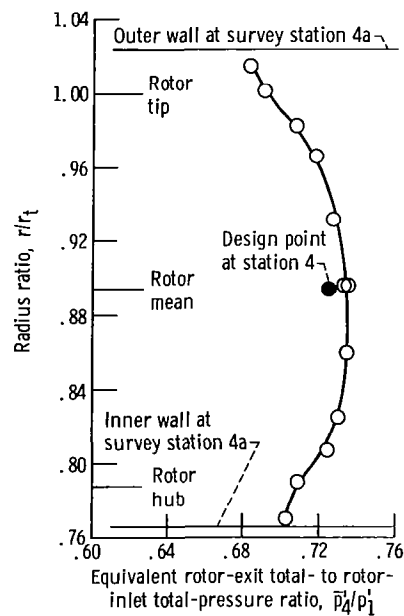

Figure 11. - Radial variation of first-stage rotor-exit total pressure at design equivalent speed and approximately design equivalent pressure ratio.

Static Pressure Distribution

The axial distributions of the static pressure at several equivalent inlet total- to rotor-exit static-pressure ratios and at design equivalent speed are shown in figures 12(a) and (b) for the tip and the hub, respectively. The design points are also shown.

Most of the available pressure drop occurs in the nozzle, but there is a positive reaction (pressure drop) across the rotor at both hub and tip sections for all pressure ratios investigated. The pressure drop across the rotor increases with the overall pressure ratio, and a small, positive radial pressure gradient occurs at both the nozzle exit and rotor exit stations.

The rotor was designed for a small pressure drop at the tip diameter, no pressure change at the mean diameter, and a small pressure rise at the hub diameter. At design pressure ratio, the tip static pressures agree fairly well with the design values. The hub static pressures, however, are higher than the design values.

At design pressure ratio, the hub and tip nozzle-exit static pressures shown in figure 12 are the same as those reported in reference 5 for the two-stage turbine. The
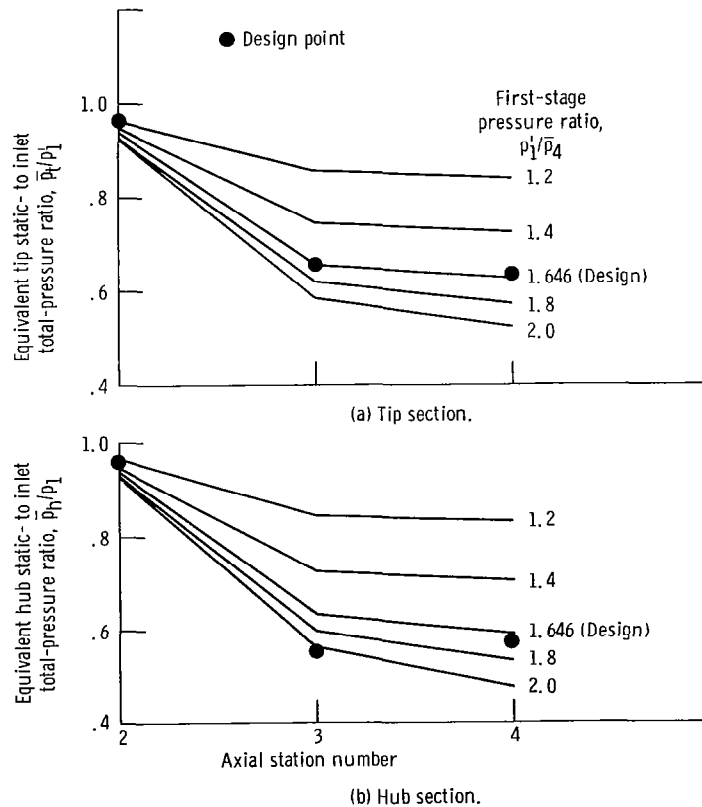

(a) Tip section.

(b) Hub section.

Figure 12. - Axial static-pressure distribution at design equivalent speed.

equivalent weight flows are also the same, as discussed in the section, Weight Flow. However, in the investigation of the inlet-manifold-nozzle assembly (ref. 4), the nozzle-exit hub and tip static pressures were nearly equal to the design values.

The first-stage rotor, which has thick, blunt, leading-edge blades and was built with a throat area 9 percent less than design, apparently interferes with the flow at the nozzle exit. This interference increases the nozzle-exit hub static pressure, which increases the average nozzle-exit static pressure $\bar{p}_3$, and reduces the nozzle pressure ratio, the nozzle-exit velocity, and the equivalent weight flow.

A similar effect was noted at the exit of the first-stage rotor in the tests of the two-stage turbine (ref. 5).

With the second-stage blading installed, the first-stage rotor-exit hub static pressure was higher than it was for the test of the first stage only. The tip static pressures were approximately the same for both configurations.

Analysis of First-Stage Performance

A velocity diagram representative of the first-stage performance was calculated from test data. The data used were for design equivalent speed and an equivalent pressure ratio $p_1'/\bar{p}_4$ of 1.664. The rotor-exit velocity was calculated from the average values of rotor-exit static and total pressures. The average values of the rotor-exit flow angle and mean-diameter blade speed were used to complete the rotor-exit velocity triangle. The rotor-inlet tangential velocity was then specified by the specific work. The rotor-inlet axial velocity was calculated from continuity. Nozzle-exit area, weight flow, and average nozzle-exit static-pressure data were used for this calculation. The resultant velocity diagram is shown in figure 13.
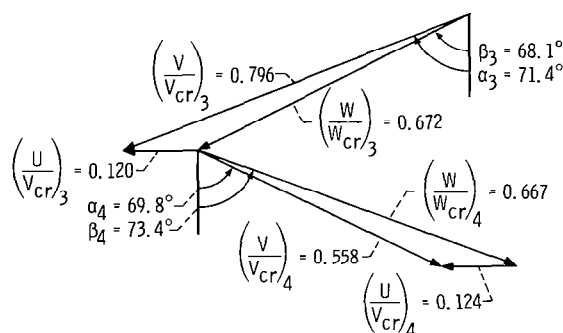

Figure 13. - First-stage mean-diameter velocity diagram calculated from test data at design equivalent speed and approximately design equivalent pressure ratio.

The axial distribution of the average static- and total- to inlet total-pressure ratios corresponding to the velocity diagram shown in figure 13 are shown in figure 14(a) and (b), respectively. For comparison, the design mean-diameter values are also shown in these figures. The value of the nozzle-inlet to feedpipe-inlet total-pressure ratio $\bar{p}'_2/p'_1$ shown in figure 14(b) was taken from reference 4.

A comparison of the actual and the design velocity diagrams (figs. 2 and 13) shows that the first-stage performance differed from design in two principal respects: (1) The nozzle-exit or rotor-inlet velocities are less than the design values, and the rotor-exit velocities are slightly higher than the design values. (2) Both nozzle-exit and rotor-exit flow angles are larger than the design flow angles.

These differences between actual and design performance are also reflected by the differences between the actual and design axial pressure distribution (fig. 14). The static-pressure distribution (fig. 14(a)) shows a static-pressure drop in the manifold rather than the design increase in static pressure. The static-pressure drop across the nozzle is less than design, and there is positive reaction (pressure drop) across the rotor. The rotor was an impulse or no static-pressure-drop design. The total-pressure variation (fig. 14(b)) shows a manifold total-pressure ratio $\bar{p}'_2/p'_1$ of 0.95 as compared with the

(a) Static pressure.

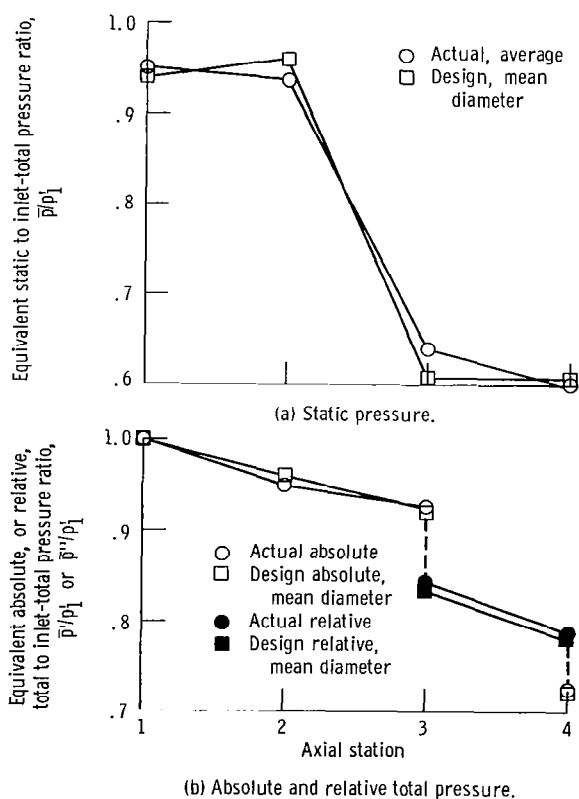(b) Absolute and relative total pressure.

Figure 14. - Comparison of design and actual mean-
diameter pressures at design equivalent speed and
approximately design equivalent pressure ratio.

design value of 0.961. However, the actual and design total-pressure ratios across the manifold-nozzle combination $\bar{p}_3'/p_1'$ are more nearly equal. They are 0.927 actual compared with 0.923 design, which indicates that the nozzle performed with less-than-design loss. The lower-than-design nozzle loss is also reflected by a higher-than-design nozzle efficiency. The nozzle efficiency is 0.94 as compared with 0.91 design. The figure also indicates that, although the reaction across the rotor is increased, the rotor total-pressure drop is approximately equal to the design value. As a result, the actual and design rotor efficiencies are about equal: they are 0.81 actual as compared with 0.80 design.

The velocity diagram and pressure data of figures 13 and 14 were used to calculate the losses in available energy resulting from the nonisentropic processes that occurred in the inlet manifold, nozzle, and first-stage rotor. The procedure used in this calculation was much the same as that reported in reference 6. The utilization of available energy, the ratio of work or loss to the ideal available energy, for the first-stage is shown in figure 15 where the actual and design values are compared.

The sum of work and leaving energy is 0.735 as compared with 0.724 design; that is, 73.5 percent of the available energy was either converted to work or made available to a succeeding stage. The closeness of these values indicates that the actual and design first-stage total efficiencies must be approximately equal. The total efficiencies were calculated to be 0.57 actual as compared with 0.563 design.

The loss breakdown in figure 15 also reflects the previously discussed high manifold loss, the counterbalancing of this loss by the better-than-design nozzle performance and a rotor loss approximately equal to design.
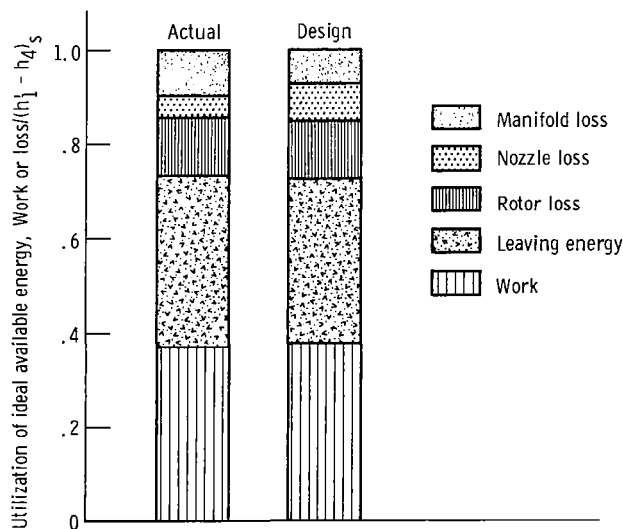

Figure 15. - Comparison of actual and design utilization of ideal available energy at design equivalent speed and pressure ratio.

18

SUMMARY OF RESULTS

The aerodynamic performance of the first stage of a 0.45-scale model of the oxygen pump-drive turbine for the M-1 rocket engine was determined experimentally. The first stage, including the inlet-feedpipe-manifold assembly, was tested over a range of speeds and pressure ratios. The working fluid used in the investigation was dry air at inlet total conditions of 600° R (333° K) and approximately atmospheric pressure. The results of this investigation are summarized as follows:

1. At design equivalent speed and blade-jet speed ratio, the first-stage static and total efficiencies were very close to the design values. The static and total efficiencies were 0.37 and 0.57 as compared with the design values of 0.375 and 0.563, respectively.

2. The equivalent weight flow at the design point was the same as that reported for the reference two-stage turbine investigation. The equivalent weight flow was 6.31 pounds per second (2.86 kg/sec) or 10.8 percent less than the design value of 7.071 pounds per second (3.20 kg/sec). This low flow is attributable to the combination of a higher-than-design inlet-manifold total-pressure loss, a large circumferential variation in manifold flow conditions, a 3.7-percent deficit in nozzle-throat area, and the less-than-design nozzle-exit velocities that were caused by a 9-percent deficit in rotor-throat area.

3. An analysis of the first-stage performance indicated that the rotor efficiency was essentially as designed, 0.81 as compared with 0.80 design. The nozzle performed better than design. The nozzle efficiency was 0.94 as compared with 0.91 design. This improved nozzle performance counterbalanced the high manifold loss. As a result, the overall efficiency of the manifold-nozzle combination was essentially as designed.

4. Velocity diagrams computed from test data differed somewhat from design. The nozzle exit and rotor exit flow angles were greater than design, principally because of the small nozzle- and rotor-throat areas. In addition, the reaction across the rotor was higher than design, also because of the relatively small rotor throat area.

Lewis Research Center,
    National Aeronautics and Space Administration,
        Cleveland, Ohio, September 20, 1967,
            128-31-02-25-22.

REFERENCES

1. Reynolds, T. W.: Aerodynamic Design-Model II Turbine M-1 Fuel Turbopump Assembly. Rep. No. AGC-8800-52, Aerojet General Corp. (NASA CR-54820), Apr. 15, 1966.

2. Stabe, Roy G.; Kline, John F.; and Gibbs, Edward H.: Cold-Air Performance Evaluation of a Scale-Model Fuel Pump Turbine for the M-1 Hydrogen-Oxygen Rocket Engine. NASA TN D-3819, 1967.

3. Beer, R.: Aerodynamic Design and Estimated Performance of a Two-Stage Curtis Turbine for the Liquid Oxygen Turbopump of the M-1 Engine. Rep. No. AGC-8800-12, Aerojet General Corp. (NASA CR-54764), 1965.

4. Stabe, Roy G.; Evans, David G.; and Roelke, Richard J.: Cold-Air Performance Evaluation of Scale Model Oxidizer Pump-Drive Turbine for the M-1 Hydrogen-Oxygen Rocket Engine. I - Inlet Feedpipe-Manifold Assembly. NASA TN D-3294, 1966.

5. Roelke, Richard J.; Stabe, Roy G.; and Evans, David G.: Cold-Air Performance Evaluation of Scale Model Oxidizer Pump-Drive Turbine for the M-1 Hydrogen-Oxygen Rocket Engine. II - Overall Two-Stage Performance. NASA TN D-3368, 1966.

6. Stabe, Roy G.; Kline, John F.; and Gibbs, Edward H.: Effect of Simulated Bearing Coolant Injection on the Performance of a Two-Stage, Velocity-Compounded Turbopump Drive Turbine. NASA TM X-1364, 1967.